Accepted Manuscript

Bending strength of CFRP laminated adhesive joints fabricated by vacuum-assisted resin transfer molding

Mahmoud R. Abusrea, Seung-Wook Han, Kazuo Arakawa, Nak-Sam Choi

PII: S1359-8368(18)30941-7

DOI: 10.1016/j.compositesb.2018.08.041

Reference: JCOMB 5871

To appear in: *Composites Part B*

Received Date: 23 March 2018

Accepted Date: 10 August 2018

Please cite this article as: Abusrea MR, Han S-W, Arakawa K, Choi N-S, Bending strength of CFRP laminated adhesive joints fabricated by vacuum-assisted resin transfer molding, *Composites Part B* (2018), doi: 10.1016/j.compositesb.2018.08.041.

Bending strength of CFRP laminated adhesive joints fabricated by vacuum-assisted resin transfer molding

Mahmoud R. Abusrea[a,b], Seung-Wook Han[c], Kazuo Arakawa[d], Nak-Sam Choi[c*]

[a] Faculty of Engineering, Cairo University, Giza 12613, Egypt

[b] Interdisciplinary Graduate School of Engineering Sciences, Kyushu University, Fukuoka 816-8580, Japan

[c] Department of Mechanical Engineering, Hanyang University, Ansan 426-791, South Korea

[d] Research Institute for Applied Mechanics, Kyushu University, Fukuoka 816-8580, Japan

* Correspondence to: Nak-Sam Choi. email: nschoi@hanyang.ac.kr

Abstract

The laminated joints used in this work were adhesive joints constructed using two dry carbon fiber halves. Some improvements were introduced to the joints to enhance their bending strength performance: stitching of the two halves together by fiber bundles and inserting extra carbon fiber covers in the joint connection. We studied three adhesive joints: a conventional basic and two improved laminated joints. All joint specimens were fabricated using a vacuum-assisted resin transfer molding (VARTM) process. The joints were evaluated with a bending test, and were compared to the bending strength of a jointless carbon fiber reinforced plastic (CFRP) laminate. Two acoustic emission (AE) sensors were placed on the specimen to monitor the fracture progresses during the test. The improved laminated joints, stitched and multiple-cover overlapped joints, showed enhanced bending strength and joint efficiency. The improvement depended significantly on the number of carbon fiber layers. The maximum increase was 24% for the stitched laminated joint of 5 layers and 58% for the multiple-overlapped joint of 6 layers, respectively. Such high joint efficiency was due to the effect of the carbon fiber reinforcement on the joints, by which many carbon fibers supported the strength in advance of reaching the maximum load point, as confirmed by AE measurement analysis.

Keywords— CFRP joints, vacuum-assisted resin transfer molding, bending strength, joint efficiency, acoustic emission

1. Introduction

Carbon fiber reinforced plastic (CFRP) composites have a significant advantage for their application in engineering structures, which is derived from their high strength-to-weight ratio [1]. They have been applied to heavy-duty structures in the aviation, spatial [2, 4], automotive [3], shipbuilding [4], and wind turbine [5] industries. These applications often involve large-scale manufacturing, and some parts are joined together from smaller components. In this case, the mechanical performance of the CFRP structure is highly dependent on the properties of the joints.

Because composite joints work as crucial load-carrying elements, their design and analysis are key processes in large-scale applications in order to accomplish light weight and efficient composite structure integration [6]. There are conventional mechanical fasteners, such as bolts, pins, and rivets, to join CFRP structures [7]. These mechanical joints are often preferred because they can be disassembled for repair and/or recycling [8]. However, drilling the holes necessary for joining the parts may induce localized damage in the composite owing to stress concentration when the joint is loaded. In contrast, adhesively bonded joints may have mechanical advantages in comparison to bolted joints because the reinforcing fibers are not cut, and thus, the stresses are transmitted more uniformly [9]. Therefore, bonded joints can provide high strength-to-weight ratio and good structural integrity [10-12].

Nowadays, adhesive joints are widely applied in many composite structures for aerospace, turbine, and ship designs [13]. These engineering structures are subjected to combinations of static, fatigue, and impact loadings. Not only conventional single-lap [9], double-lap [14], and stepped [15] adhesive joints, but also improved adhesive joints have been studied to ameliorate the mechanical performance of adhesive composite joints. For instance, Löbel et al. [16] enhanced the tensile strength by introducing z-pinning into CFRP double-lap joints. Another approach for adhesive joint improvement was reported by Mouritz et al. [17], who placed spiked metal sheets in the bond-line to facilitate mechanical load dispersion. Furthermore, stitching was proposed as a technique for reinforcing laminated joints. Dransfield et al. [18] and Heß et al. [19] clarified that the stitching enhanced the fracture toughness of laminated composites under peel loading. Kim et al. [20] made some stepped-lap joints as a function of the number of steps,

joint length, and edge angle of the adherends, and showed a considerable improvement in the fatigue performance by increasing the number of steps and the edge angle.

Vacuum-assisted resin transfer molding (VARTM) has been recognized as a useful fabrication technique to make large-scale CFRP structures with adhesive joints [19-20]. We developed this technique in our laboratory to apply it to the fabrication of wind-lens parts for offshore wind power applications [10-12]. Using this VARTM technique, several novel adhesive bonded joint structures were fabricated based on the stacking of carbon-fiber layers to evaluate their tensile strength performances. The first type of joints was constructed from partially unmolded dry carbon-fabric layers [12]. Tensile testing indicated that the novel double-lap joints were more than twice as strong as a classical double-lap joint. The second type of joints was made from two pairs of layers [10]: one pair comprised two mating dry carbon fibers, and the other pair consisted of a dry carbon and a pre-molded CFRP fabric. The laminated adhesive joint from the two dry carbon fibers achieved a higher tensile strength than the other paired joint. Multi-overlapped joints showed the best performance, equivalent to 85% of the tensile strength of a jointless CFRP. Furthermore, a stitching was applied to the above joints [11]. The stitching improved the tensile strength of the former joint, constructed of two dry carbon fibers, whereas it decreased the tensile strength of the latter joint. The novel adhesive joints have been evaluated only in terms of tensile strength. In real working situations, the adhesive joint structures are commonly subjected to bending moments caused by a strong wind force, and thus their bending performance need to be extensively investigated.

In this study, a CFRP laminated adhesive joint, referred to as a basic laminated joint (BLJ), is fabricated using VARTM, as schematically illustrated in Fig.1. This joint is constructed of two mated dry carbon fiber halves. Two modifications are introduced to the joint. One is the application of a stitching to the basic laminated adhesive joint, i.e., a stitched laminated joint (SLJ) and the other is the addition of carbon fiber covers onto the conventional adhesive joint, i.e., a multiple-cover laminated joint (MCLJ). The three types of joint specimens are cured and then subjected to three-point bending tests with acoustic emission (AE) measurement. The performances of the adhesive joints are characterized in terms of bending strength in comparison to the jointless CFRP laminates. The objective of this work is to accomplish improved bending strength in the joint types. Important fracture mechanisms of the joints are clarified by detection of AE measurement data in combination with optical and scanning electron microscopy.

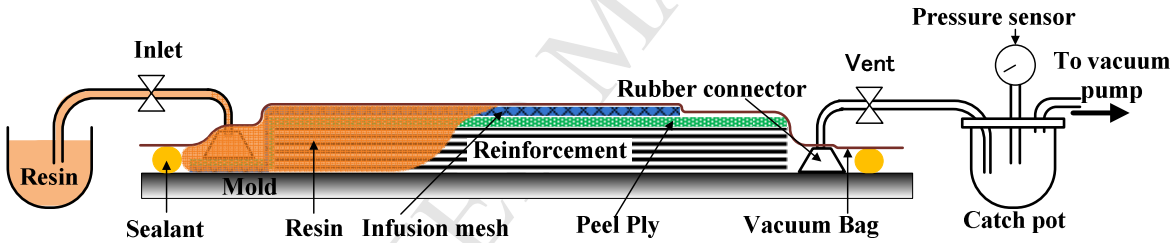

Figure 1. Schematic diagram of the vacuum-assisted resin transfer molding (VARTM) process

2. Experimental method

2.1. Materials and Fabrication

The composites and adhesive joints consisted of carbon fabric, as presented in Table 1, and a resin (Denatite XNR/H 6815, supplied by Nagase & Co.). The resin was a mixture of XNR6815 and XNH6815 with a weight ratio of 100:27. The viscosity of the resin mixture at 25 °C was 260 MPa•s prior to the resin infusion in the VARTM process.

Table 1. Detailed information of the carbon fabric [21]

Carbon fiber designation	Style	No. of filaments	Weight	Density	Thickness	Tensile strength	Tensile modulus	Elongation
			g/m^2	g/cm^3	mm	MPa	GPa	%
TRK976PQ RW	UD 1M	12,000	317	1.82	0.33	4,900	253	1.9

The laminated joints proposed in this work are composite adhesive joints constructed of two mating dry carbon halves, which were stacked in a pre-determined order prior to the VARTM process [10-12], as schematically shown in Fig. 1. Three joint types were adopted in this work. The adhesive joint constructed of only two mating dry carbon halves was the basic original type (see BLJ in Fig. 2a). The joint length was 40 mm, with total specimen length of 80 mm. The fiber volume fraction measured for the joints was approximately 62%. One improvement to this joint was made by applying a stitching technique. Fig. 2b shows the stitched laminate joint (SLJ). We conducted stitching with carbon bundles of the same carbon fiber type, which were applied perpendicularly to the plane of the laminate [18-19]. Abusrea and Arakawa [11] showed a weakened stepped joint in which stitching was applied; the tensile strength of this stitched stepped joint was 26% lower. However, it showed improved tensile strength when the stitching was applied to the dry carbon-to-dry carbon joint state. The other improvement was made by adding carbon fiber covers of 40 mm in length, which had been prepared beforehand by sectioning the carbon fiber layers. Each carbon fiber cover was put on the contact region between the end parts of two mating dry carbon fiber layers. After finishing the VARTM process [10,11], the inserted carbon fiber covers may reinforce the interphase layer between the two overlapping carbon halves, and may alleviate the stress concentration at the fiber ends of the carbon halves. This joint type is named the multiple-cover-overlapped laminate joint (MCLJ) (see Fig. 2c). We applied four different numbers of carbon fiber layers to all joints. We chose 5, 6, 7, and 10 carbon fiber layers, as these numbers are common in the industrial use. For the basic type of a laminated joint, two different cases were made: a normal BLJ and a “shifted” basic laminated joint (shifted BLJ). For the normal BLJ, the six and ten carbon fiber layers were stacked “correctly” at their right positions; that is, there was no gap between the fiber ends (Fig. 2a). For the shifted BLJ, the five and seven carbon fiber layers were a bit shifted to form a gap between the fiber ends (Fig. 2b). Because a shifted placement of the carbon fiber layer may be conducted during mold preparation for this kind of adhesive joint fabrication, the shifted BLJ was used to examine the effects of such shifting on the final product quality in terms of thickness variation, and on the mechanical performance in terms of bending strength.

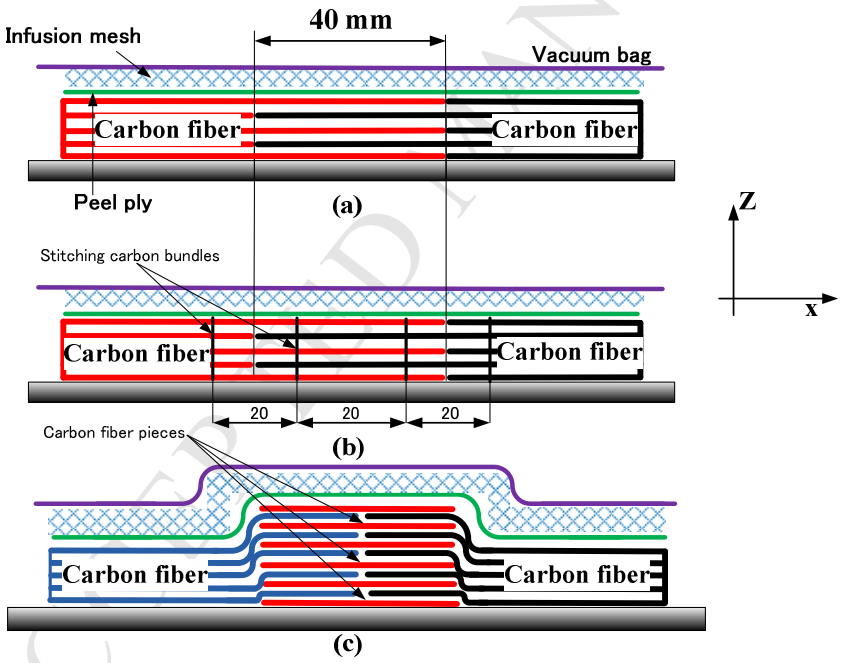

Figure 2. (a) Basic laminated joint (BLJ). (b) Stitched laminated joint (SLJ). (c) Multiple-cover laminated joint (MCLJ)

All CFRP fabrics and joints were fabricated using the VARTM process shown in Fig. 1. Composite joint fabrication with the VARTM involved three steps: mold preparation, filling with resin, and curing. In the initial step, the mold surface was treated with a mold release agent (TR High-Temp). The dry carbon fiber layers were stacked on the mold according to the desired joint types. The stacked carbon fiber layers were covered by a peel ply. Both the chemical agent and peel ply were applied so that the final composite joints could be released readily after curing. Then, an infusion mesh was applied over the peel ply, providing two main functions: promoting resin flow and facilitating the

drawing of resin into any voids before resin curing. Two rubber connectors and spiral tube pieces were placed as the inlet for infusion and the vent for air and excess resin elimination, respectively. The whole package was enclosed in a vacuum bag and tightly sealed with gum tape sealant. Finally, two external hoses were connected to the inlet and vent. One was connected to the resin source and the other to a vacuum pump. To ensure a leakage-free mold, a sealing test was performed in accordance with an appropriate procedure before resin filling. After the resin filled the stacked fiber joint reinforcements on the mold and excessive resin exited the vent, the inlet was closed and the vent was left open for 24 h until the resin cured. Details of the VARTM process are explained in the previous papers of the authors [10, 11].

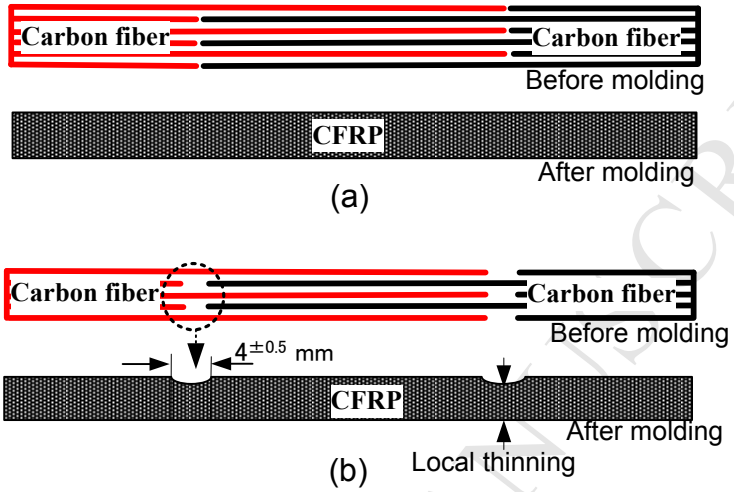

Figure 3. Schematic drawing before and after molding for the (a) normal basic laminated joint (normal BLJ) and (b) shifted basic laminated joint (Shifted BLJ).

2.2. Mechanical testing with AE measurement

The nominal bending strength was measured [24] to evaluate the joints' mechanical performances. The cured CFRP joints were sectioned to form specimens for the three-point bending tests, with the geometry shown in Fig. 4. Five specimens were prepared for each test condition. The span (L) and the width (W) of the test specimens were 50 mm and 12.7 mm, respectively. The thickness (t) of the joints was varied according to the joint types in Fig. 2, and thus, they were measured for the individual joint type in advance of the tests. The thickness (t_o) of the unjointed part of the test specimens was also measured. During the test, each specimen was monitored by AE measurement. The bending test was carried out at room temperature with a universal testing machine (Zwick 250, Test Xpert, version 11) with a crosshead rate of 3 mm/min. The fracture processes were examined in real time using two AE sensors (micro30, Physical Acoustic Corp.), which were attached to the bending specimen using vacuum grease and a mechanical fixture. The two AE sensors were put 46 mm apart, and each one is 23 mm distant from the specimen center. They were placed in such positions close to the joint ends. A two-channel AE detection system (MSTRAS 2001, Physical Acoustic Corp.) was used to record the AE data, and the AE measurement conditions were a pre-amp of 40 dB, a threshold level of 40 dB, and a sampling rate of 4 MHz. The threshold was positioned at a comparatively high level so as to filter the noisy sounds coming from other emission sources. A band-pass filter under software control (pass range from 1 kHz to 1 MHz) was used for signal gain at specific frequencies. Three AE parameters were investigated: amplitude, energy, and frequency spectrum of the AE signals. The AE analysis may provide a way to identify and differentiate fracture sources [22,23]. In agreement with Yoon et al. [22], we ascertained that the distance between the sensor and the crack location was close enough to measure the AE characteristics. Considering the attenuation problems at high frequencies, we focused primarily on frequency bands below 400 kHz for verification of the fracture mechanisms. A fractographic analysis was also performed on the damaged specimen surface and/or the fracture surface through observation by optical and scanning electron microscopy (SEM).

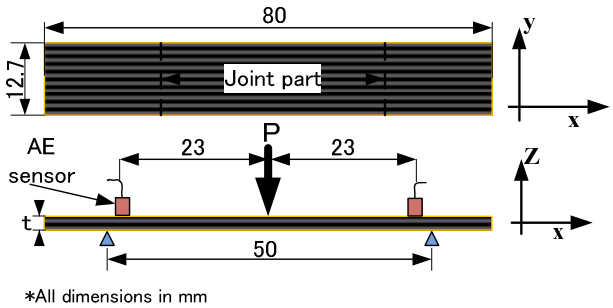

Figure 4. Illustration of an adhesive joint specimen under the three-point bending test with acoustic emission (AE) monitoring.

2.3. Data reduction of the adhesive joints under the bending test

The maximum load taken during the bending test in Fig. 4 is used to evaluate the mechanical performance of the composite adhesive joints. It is reasonable that the joint performance should be compared with the bending strength of the jointless original composite laminates. In this respect, the "nominal" bending strength σ_1 for every joint type can be calculated using

$$\sigma_1 = 3PL/2Wt_o^2, \quad (1)$$

where P is the maximum load value obtained from the load-deflection curve of the respective joint types , L the span length, W the specimen width, and t_o the thickness of the unjointed ligament part. The nominal bending strength assumes that the adhesive joint has a thickness equal to the unjointed ligament part. However, the thicknesses of composite adhesive joints vary significantly according to the adhesive joint types, and can generate a large variety of actual bending strength. Thus, a joint efficiency (η) for the various joint types is evaluated with reference to the bending strength (σ_o) of the jointless original composite laminate and can be determined by a simple equation

$$\eta = \sigma_1/\sigma_o \quad (2)$$

For the shifted BLJ, the nominal bending stress (σ_2) on the surface at the thinned section of a joint specimen is given by

$$\sigma_2 = 3Pb/Wt_c^2, \quad (3)$$

where b is the distance between the support roller and the thinned section, and t_c is the thickness of the thinned part.

3. Results and discussion

3.1. Thickness profile behaviors of the joint specimens

Table 2 lists the thickness measurement data obtained for the normal BLJ. The average thicknesses were 1.83 and 3.04 mm for 6 and 10 layers, respectively. The minimum thickness and the maximum deviation were also measured for evaluating the product quality. The thickness deviation ranged up to 2.8% for 6 layers and up to 3.5% for 10 layers. For the shifted BLJ, the average thicknesses for 5 and 7 layers were 1.46 and 2.02 mm, respectively, as listed in Table 3. The thickness deviation was as high as 23%. The low minimum thickness and the large deviation indicate a bad quality that may lead to weaker strength for the thinned part of the shifted BLJ specimens. Several previous papers mentioned that the thickness variation was one of the geometrical parameters that exerted a negative influence

on the performance of adhesively bonded joints [24]. For example, the local thinning owing to thickness variation could affect the stress concentration, strain inhomogeneity, and crack initiation. Ribeiro et al. [25] calculated the stress distributions along a single lap adhesive joint to show a rapid increase in stress gradients around the overlapped edges. Jensen et al. [26] showed a strain inhomogeneity, reaching nearly 20% of the mean strain value, in composite laminates under a transverse load.

Figure 5 compares the specimen thickness profiles along the specimen lengthwise direction for the three kinds of joints (normal BLJ, SLJ, and MCLJ) with the same 6 fabric layers, and also for an "ideal" 6-layer jointless CFRP. The stitched joints showed higher thickness deviation, especially at the stitched sites. The thickness deviation was about ±0.45 mm. Much greater thickness increase at the joint part was observed for the MCLJ. The thickness at the joint part along the joint length of 40 mm was measured to be 3.3 mm on average, which was almost twice the thickness of the jointless CFRP. This was because the number of carbon fiber covers generated additional thickness, exceeding the initial thickness of the adherend constructed with the original number of carbon fiber layers. This large variation in thickness appeared along the upper surface profile of the joint part because all carbon fiber layers, including the additional covers, were placed on a rigid flat surface of the mold, as illustrated in Fig. 2c.

Table 2. Thickness profile data for normal BLJ

	Thickness, mm	minimum thickness, mm	thickness deviation, % max
6 layers	1.83(0.04)	1.78	2.8
10 layers	3.04(0.07)	2.93	3.5

Table 3. Thickness profile data for shifted BLJ

	Thickness, mm	minimum thickness, mm	thickness deviation, % max
5 layers	1.46(0.08)	1.15	21
7 layers	2.02 (0.08)	1.55	23

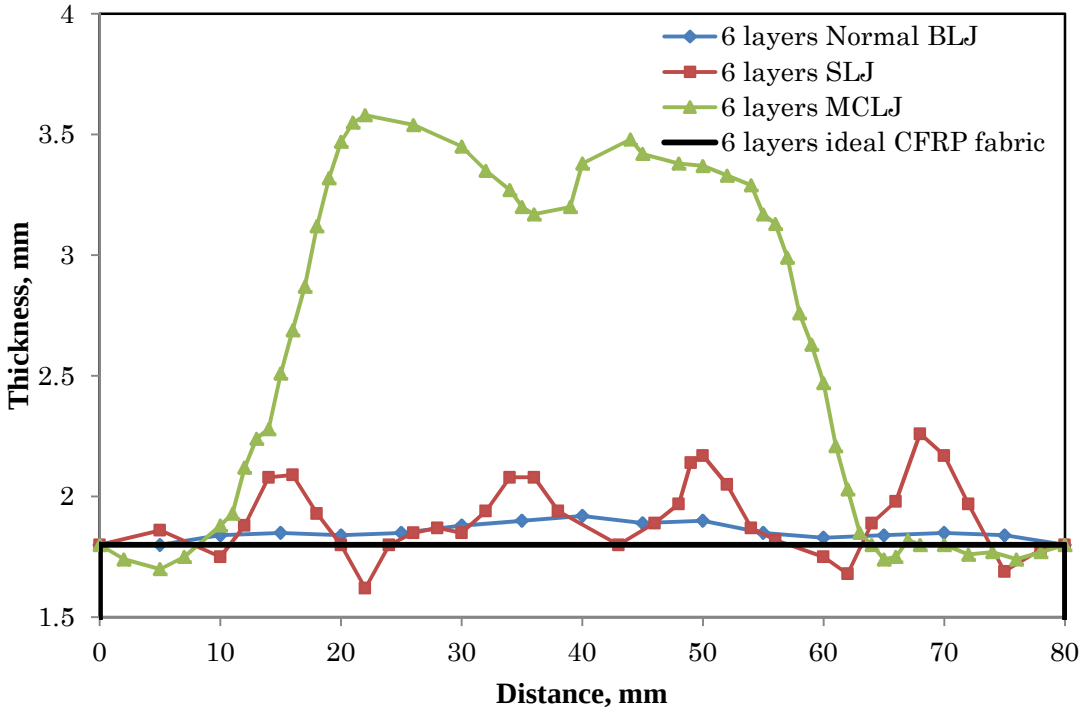

Figure 5. Typical thickness profiles for the three types of joints and the jointless CFRP

3.2. Bending strength and fracture processes of basic laminated joints (BLJs)

Figure 6 shows the obtained nominal bending strengths for the normal and shifted BLJs. For the normal BLJ, the average bending strengths for 6 and 10 carbon fiber layers were 554 and 870 MPa, respectively. It is to be noted that a larger number of layers caused bigger bending strength. The tensile stress concentration at the fiber end in the surface layer under bending load might induce a similar crack initiation for both numbers of fiber layers. However, with a higher number of fiber layers, its propagation seemed to be significantly hindered by the numerous neighboring reinforcing fibers. Lower bending strengths were recorded for the shifted BLJ in comparison to the normal BLJ. During the VARTM process, the shifted BLJ had a finite gap filled with resin between the fiber ends, and the gap region in the joint was shrunk into a concave shape during curing. The thickness at the concave cross-section was measured to be 21% smaller than the normal BLJ. Such large concaveness must have caused a severe notch effect, i.e., weakened bending strength. The shifted BLJ with a higher number of layers, which had deeper concaveness, showed a much larger decrease in bending strength , as depicted in Fig. 6.

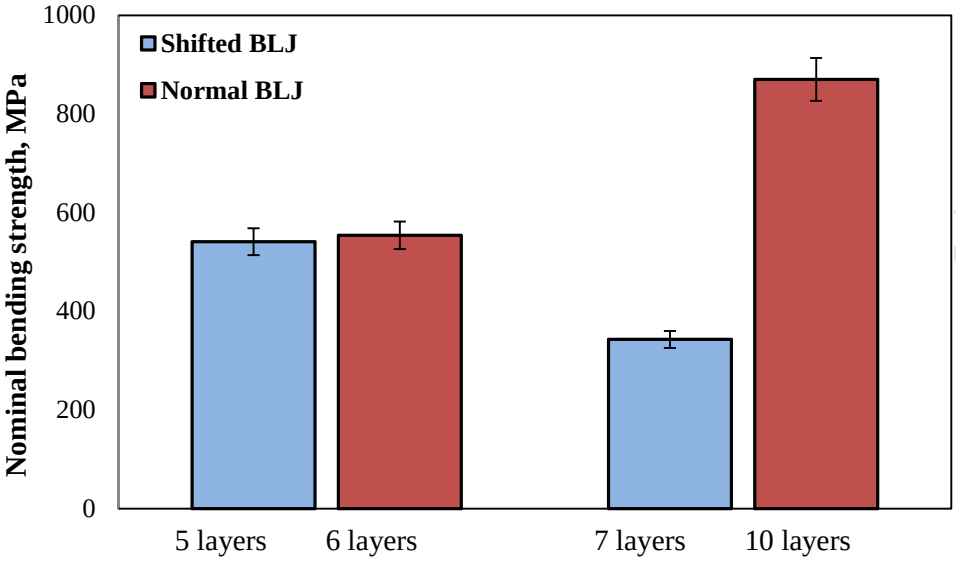

Figure 6. Bending strength results for normal and shifted BLJ specimens

Such bending strength behaviors may be clarified by the AE analysis in combination with microscopic fractography. Figure 7 shows a typical bending stress curve versus time for the normal BLJ specimen of 6 layers, which was recorded together with the accompanying AE amplitudes. With the increasing displacement, the load began to increase, then dropped abruptly just after reaching the peak, and finally decreased very slowly. Low amplitude emission occurred from the low level of load, whereas big amplitude emission began to be generated at around 65% of the peak load, and then appeared intermittently until the peak load. High amplitudes may correspond to fiber breakages while low amplitudes may arise from cracks in the resin and/or interface between fiber and matrix, as ascertained in ref. [22,23]. In this sense, it was confirmed that for normal BLJ some amount of reinforcing fibers were broken before reaching the bending strength. However, only low amplitudes arose with the rapid load drop just after the peak. After finishing the large load drop, very high amplitudes were generated again, following a mild AE behavior.

The typical bending stress behavior for the shifted BLJ of 5 layers with accompanying AE amplitudes is shown in Fig. 8. Clear differences from the normal BLJ appeared in this figure. The peak load level for the shifted BLJ was a bit lower, and the load drop proceeded in several steps and times. Big amplitude emissions began to occur at a quite high level of 90% of the peak load, and they were sustained for a considerably long time with a slow decrease in load after the peak load. This behavior shows that around the peak load the reinforcing fibers were broken in a very different process from the normal BLJ. After passing such strong emission period, the load dropped down to around 50% of the peak load.

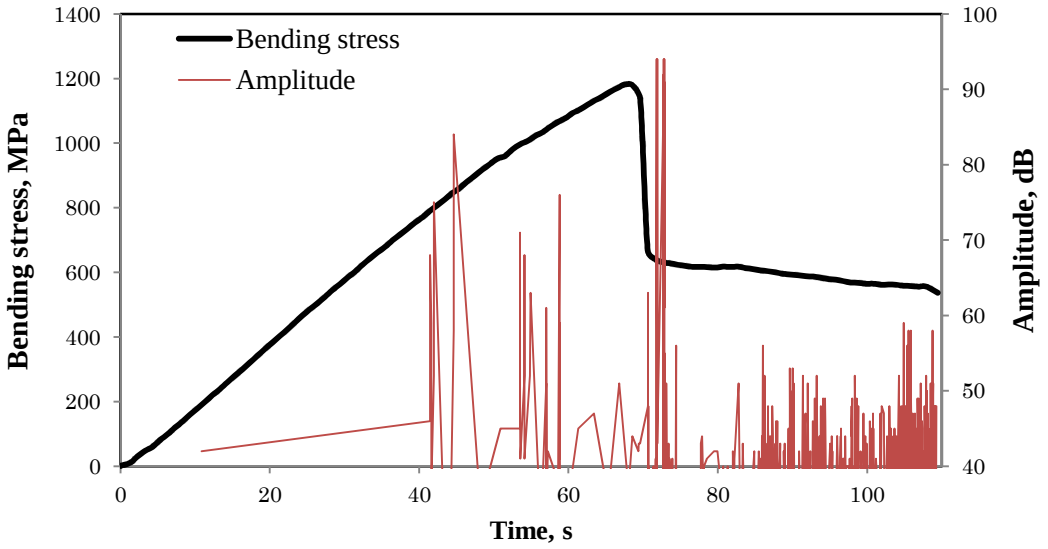

Figure 7. Typical bending stress curve versus time with accompanying AE amplitudes for a normal BLJ specimen constructed of 6 fiber layers.

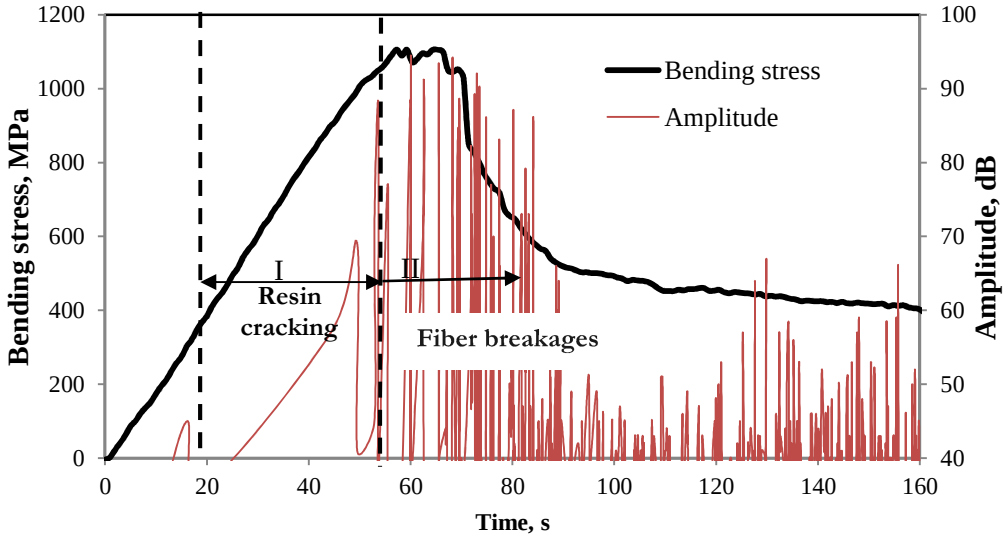

Figure 8. Typical bending stress-time curve with accompanying AE amplitude for a shifted BLJ specimen of 5 fiber layers.

Fractographs taken for the normal and shifted BLJs were analyzed as shown in Fig. 9. For the normal BLJ specimen, a tensile bending fracture occurred along the center line of the specimen, 20 mm distant from the joint ends, and it induced many fiber breakages as revealed in the SEM observation (see Fig. 9a). It is noted that the tensile bending stress at the joint end of this specimen, calculated by equation (3), approached only about 80% of the peak stress at the middle of the specimen. The shorter the distance from the specimen center to the joint end was, the larger the tensile stress arising at the joint end. Thus, short joints can cause a fracture at the joint end because the joint ends have a weaker strength by lack of reinforcing fibers, which may lead to a lower joint strength than the long joints used in this study. In contrast, the shifted BLJ showed a different failure behavior as confirmed by optical

microscopic observation (see Fig. 9b). A resin crack was initiated at the joint end where the local thinning had been formed, as presented in Table 3, and proceeded in the loading period without observed fiber breakages along the laminate interface. This phenomenon was also confirmed in accordance with the low amplitude distribution until about 90% the peak load, as shown in Fig. 8. The shifted BLJ can arouse a peak tensile stress at the bottom of the concave part where the local thinned section was located. For this stress analysis, a stress concentration effect should be considered based on the measured notch length a and notch tip radius ρ_t by the following equation:

$$Stress\ concentration\ factor\ (K_t) = \frac{Highest\ stress\ (\sigma_m)}{Nominal\ stress\ (\sigma_2)} = \left[1 + 2 * \sqrt{\frac{a}{\rho_t}}\ \right] \quad (4)$$

The values of K_t for the shifted BLJ specimens of 5 and 7 layers may be estimated as 1.34 and 1.45, respectively. The high stress values beyond the stress at the center of the joint specimen must have caused such crack initiation at the local thinned position, leading to the low bending strength of the shifted BLJ specimens. However, many fiber breakages seemed to occur just around the peak load in the process of macroscopic delamination in the joint part, as indicated by the strong amplitude emissions shown in Fig. 8. It is thought that the collapse mechanism of the shifted BLJ specimens was significantly associated with not only resin cracking and delamination in the loading stage but also with fractures of the reinforcing fibers in the joint.

Fracture mode detection using AE frequency analysis was performed during the entire loading stage. We classified the AE features according to the fracture mode based on the previous study results in which low spectral features, below 160 kHz, corresponded to resin fractures, intermediate spectral features in the range of 160–240 kHz corresponded to matrix–fiber mixed fractures, while high spectral features, above 240 kHz, were associated with fiber fractures [22,23].

Figure 10 shows the percentage data of AE energy accumulated until just after the peak load point, according to the above mentioned frequency bands for all specimens. Different fracture behaviors were identified for the normal and shifted BLJs. It was found that for the normal BLJ, the AE energy spectra occurred mostly (85–90%) in the high frequency band (f > 240 kHz). Thus, the dominant fracture mode was obviously fiber breakages. The shifted BLJ showed that most of the resin cracking took place in the overall loading stage, because a high fraction (50–65%) of the AE energy spectrum occurred in the low frequency band (f <160 kHz). A significant portion (20–30%) of the fiber breakages was also shown in this joint, which should have arisen through the delamination process in the joint part, as confirmed by the strong emissions in Fig. 8.

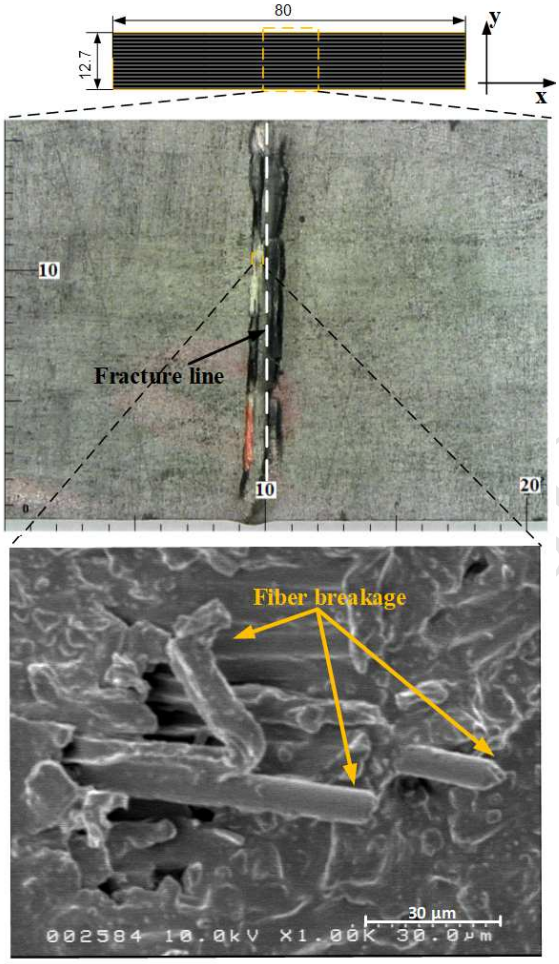

(a)

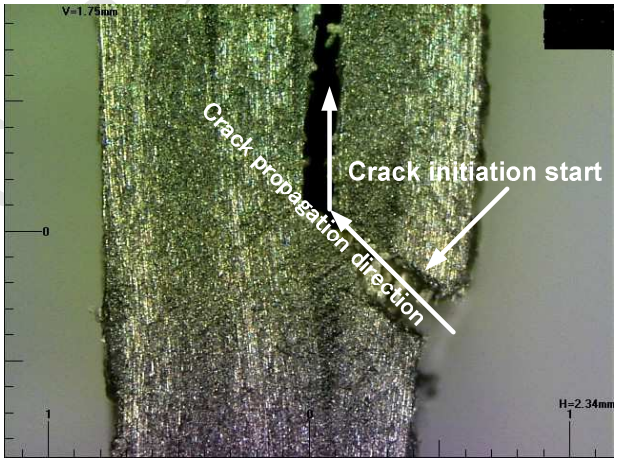

(b)

Figure 9. Typical optical microscopy and SEM micrographs for the fracture of (a) normal BLJ with 6 layers and (b) shifted BLJ with 5 layers

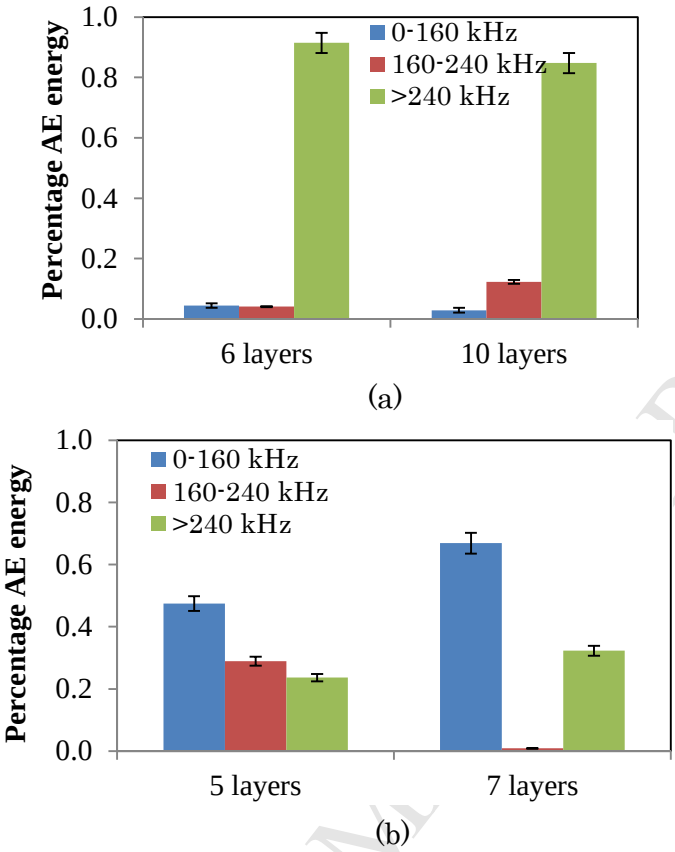

Figure 10. Percentage data of AE energy for (a) normal BLJ and (b) shifted BLJ according to the three frequency bands

3.3. Bending strength and fracture processes of stitched laminated joints (SLJ)

For the SLJ, compared with the BLJ, an improved bending strength appeared. The nominal bending strength of a SLJ with 6 layers (see Fig. 11) was 1405 MPa, showing a high increase of 54%. A very high increase of 145% was achieved by the SLJ with 5 layers. The increase in bending strength by the stitching depended on the number of laminated layers. The stitching showed a large effect on the joint efficiency calculated by equation (2). A high efficiency was recorded for the SLJ specimens depending on the number of layers (see Fig. 11 in comparison to Fig. 6). Interestingly, the SLJ with 5 layers showed a high joint efficiency, exceeding 100%, which means that its endurance capacity was greater than the bending strength (around 1500 MPa) of the jointless CFRP laminate itself.

As seen in Fig. 5, local thinned profiles, thus notches, were formed at the stitched sites of the SLJ. With this bending test, the fracture started to propagate not at the joint ends but in the middle of the joint parts. The macroscopic crack started at one of the notches formed by stitching. The stitches, which were applied across the carbon fiber layers, should have hindered the crack initiation along the interface between the fiber layers at the joint ends. Abusrea and Arakawa [11] confirmed through a tensile test that the stitching improved the tensile strength of a staircase adhesive joint owing to the bidirectional fiber structure with additional perpendicular reinforcement function. Plain and Tong [27] used a stitching technique to improve the mode I and II fracture toughness for laminated composites. Velmurugan et al. [28] showed some retarded crack initiation and delayed crack growth when a stitching was applied to a cylindrical shell subjected to axial compression. Regarding bending load, Chung et al. [29] found that the stitching improved the strength of CFRP and KFRP by 25%. Adanur and Tsao [30] reported an improvement in the flexural properties of KFRP and CFRP, even when they were stitched at a comparatively low density. The through-thickness stitching performed by many researchers improved the mechanical performances of the laminated adhesive joints. Aymerich et al. [31] reported, for single-lap composite joints, that the stitching prolonged the duration of the crack propagation phase under fatigue loading. Sawyer [32] also confirmed an improvement in static failure strength, up to 38%, by using a stitching into single-lap bonded composite joints. Jain et al. [33] also showed that the stitched adhesive joints achieved a large increase, of 36.5%, in the peak load compared to the unstitched

laminated joints manufactured by the RTM technique.

With the increase in thickness and/or layup number, the average bending strength decreased to a low value of 1144 MPa for the 7-layer SLJ. AE energy spectra and SEM analyses were conducted for the SLJ. Figure 12 shows typical percentages of AE energy in the three frequency bands for SLJs with 5, 6, and 7 layers. The SLJ generated a higher percentage (approximately 74%) of AE energy in the high frequency band (>240 kHz). This behavior was quite consistent for joints with various layup numbers. Such behavior of high frequency emissions indicates that, for the SLJ type, fiber breakages dominated the fracture process up to the peak load. The effectiveness of the stitching in the bending strength decreased considerably at higher thicknesses. A reason of the low strength with thick SLJ seems to be related with the fact that many reinforcing fibers and stitched yarns were broken in the loading stage prior to the peak load. This can be attributed to the fact that, with increasing layup thickness, the stitching formed larger notches partly filled with resin in the skin layer [11]. This fracture behavior was confirmed by a SEM image analysis, where many fiber breakages appeared in the fracture initiation region for the thick SLJ specimens with 7 layers.

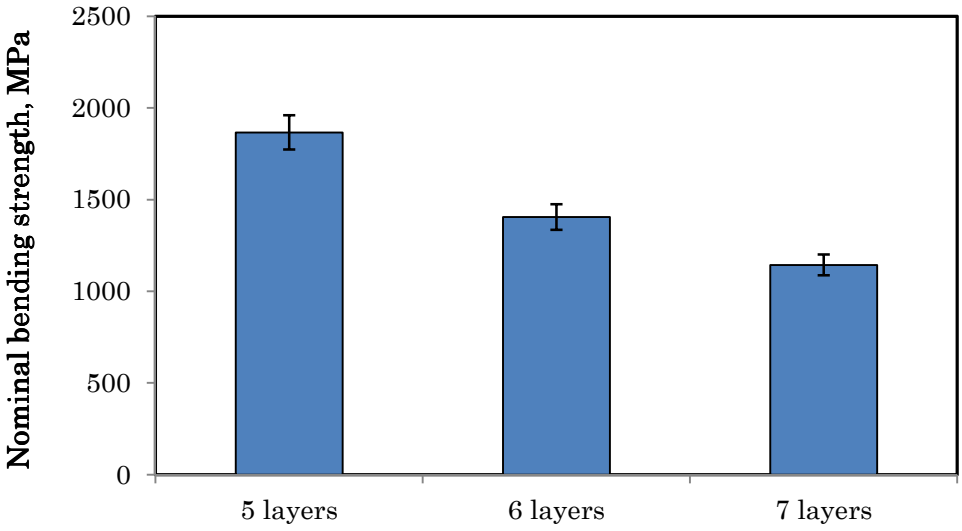

Figure 11. Nominal bending strengths for SLJ with various layup numbers in the joint

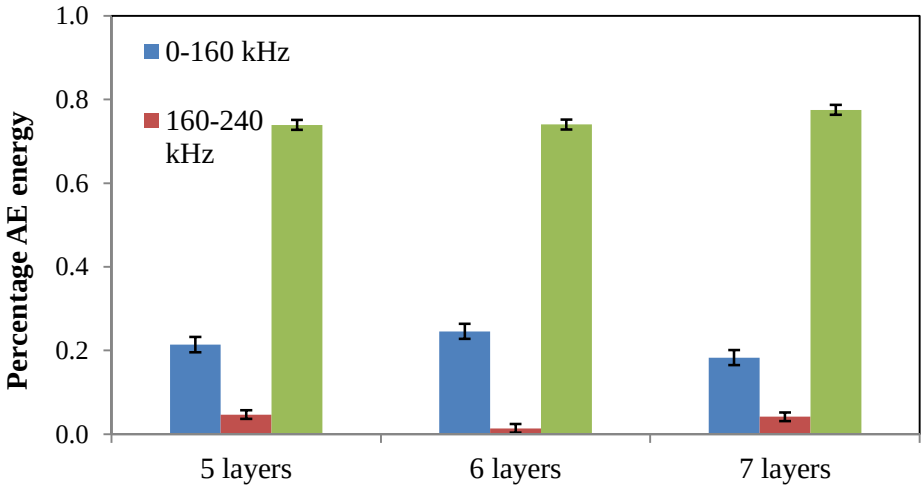

Figure 12. Percentage data of AE energy for SLJ according to the three frequency bands

3.4. Bending strength and fracture processes of multiple-cover laminated joints (MCLJ)

The MCLJ achieved much higher nominal bending strength than the BLJ. As shown in Fig. 13, the MCLJ with 6 layers had a bending strength of 2.33 GPa, which represented the maximum bending performance among all the tested MCLJ types. The strength value indicated a drastic increase, of 321%, compared to the normal BLJ, and a considerable increase, of 66%, compared to the SLJ. The MCLJ with 10 layers showed a decreasing value, of 1.29 GPa, but still larger than the SLJ. The increase in bending strength for the MCLJ can be explained by simple stress analysis: the insertion of seven extra carbon fiber covers, as illustrated in Fig. 2c, produced a thick laminated joint, which could work as a multiple-bonded double lap joint (DLJ). Because the MCLJ specimen was manufactured with the VARTM method, the joint part smoothly changed to the thin ligament adherend by filling the resin into the corner between the thick joint part and the thin adherend. The thickness of the joint part was almost twice as large as that of the adherend. In this case, the tensile stress at the bottom surface of the joint part is calculated to be one-fourth of that for the corresponding BLJ according to equation (1) under the same bending load. The macroscopic fracture shown in Fig. 14 proceeded at the center line of the joint part, which was also observed for the normal BLJ specimen (Fig. 9). If the same material strength is assumed for both the BLJ and MCLJ, the bending strength of the MCLJ should be four times as large as that of the BLJ. This agrees well with the above bending strength result of approximately 4.21 times larger than the BLJ. The small mismatch of the bending strength data between measurement and calculation might be due to the fluctuating deviation in the thickness of the joint part (see Fig. 5).

The thickness change from the adherend to the joint part was measured as shown in Fig. 5, which should induce a peak stress concentrated at the local site just where the joint began from the adherend. However, all the fracture events only occurred at the middle of the joint part, which indicates that the peak stress at the boundary site of the joint part did not reach the tensile strength of the MCLJ specimens. The peak stress site and the fracture initiation might occur probably at the end of the joint part by decreasing the length of the MCLJ part in comparison to the test span. In this case, the bending strength mechanisms should be different because of the fracture process arising at the joint ends.

The macroscopic fracture along the center line of the joint part was similar for all the MCLJ specimens with various layers adopted in this study. The MCLJs with 5, 7, and 10 layers showed lower bending strengths than the MCLJ with 6 layers. The low bending strength of the 5-layer joint might be predicted with the simple stress theory of equation (1), above stated for the 6-layer joint, in that the 5-layer joint had an average thickness larger by about 10% than that expected from the normal layup thickness. The rather thicker 5-layer joint was due to the larger resin infiltration in the VARTM process than that for the 6-layer joint. However, the decreasing bending strength of MCLJs with 7 and 10 layers could not be clarified with the simple stress theory, but be attributed to a large defect formation in the thick layup joints. For the 7- and 10-layer joints, additional fiber covers were inserted between the layers, causing a much thicker joint part, which could contain bigger voids during the VARTM process. The existence of critical large voids might induce an easy fracture of the thick MCLJ. Figure 15 shows typical percentages of AE energy in the three frequency bands for MCLJs with 5, 6, 7, and 10 layers. Most MCLJ specimens emitted a high percentage (60–98%) of AE energy in the high frequency band (>240 kHz). This implies that fiber breakages were clearly dominant in the fracture process until the peak load, as confirmed again in the SEM observation of Fig. 14. The bending strength behaviors in Fig. 13, which largely depended on the thicknesses of the MCLJ, have been associated mainly with a fracture procedure of the carbon fabric during the loading stage.

The joint efficiencies for all the types of laminated adhesive joints were calculated using equation (2) in comparison to the jointless CFRP laminates as summarized in Fig. 16. The average bending strength of the jointless CFRP was measured to be around 1500 MPa. This value was obtained for the same fiber and resin and the same manufacturing technique (VARTM). For a normal BLJ, the joint efficiency was distributed in the range of 24%–58%. For a stitched LJ, the joint efficiency was the largest (124%) with the 5-layer joint; however, over 5 layers, it was significantly reduced. Excellent joint efficiency, exceeding 100%, was also shown for the MCLJs with 5–7 layers. The best efficiency among all the joint types was obtained with the 6-layer MCLJ.

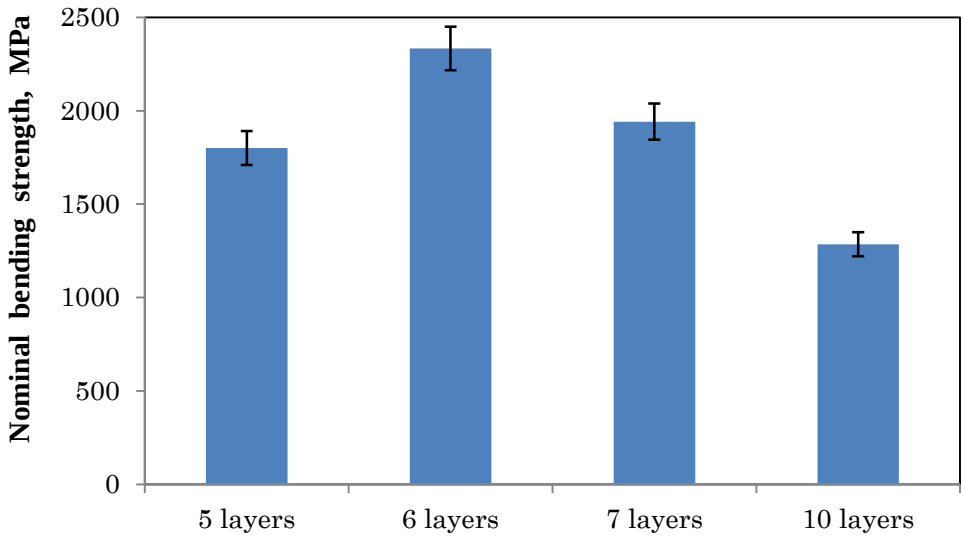

Figure 13. Nominal bending strengths for MCLJ with various layers in the joint

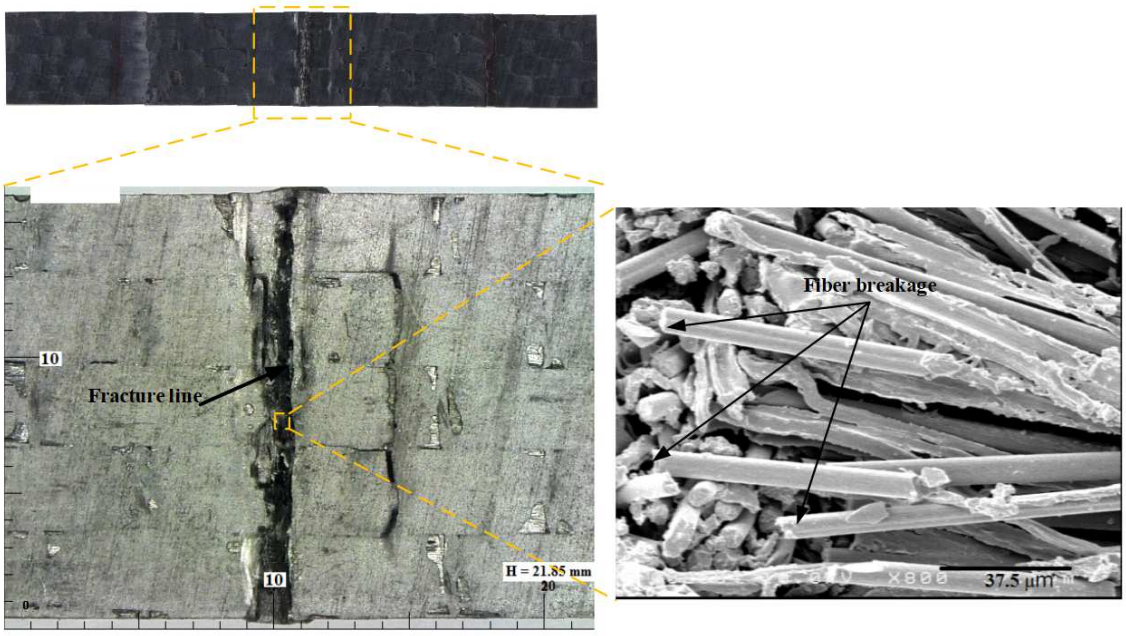

Figure 14. Typical optical and SEM photographs for the fracture of MCLJ with 6 layers

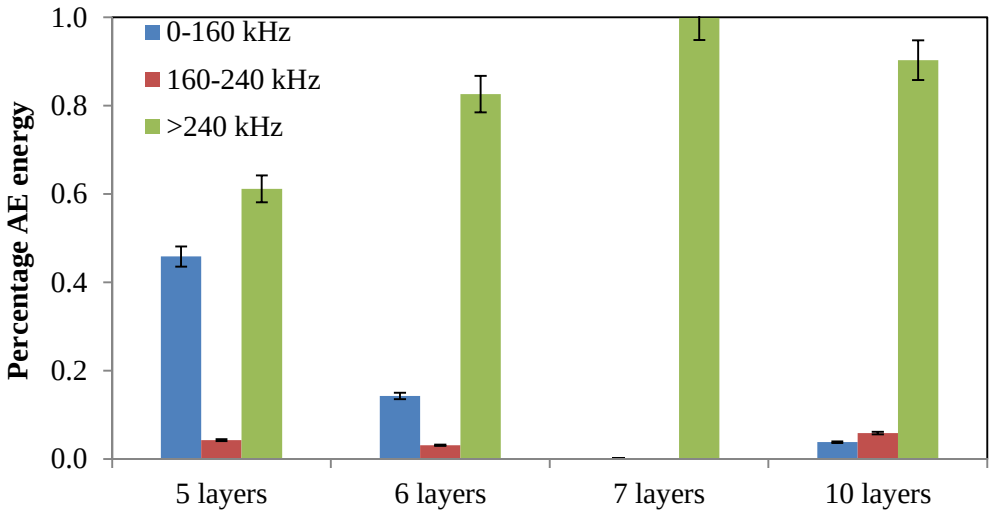

Figure 15. Percentage data of AE energy for MCLJ according to the three frequency bands

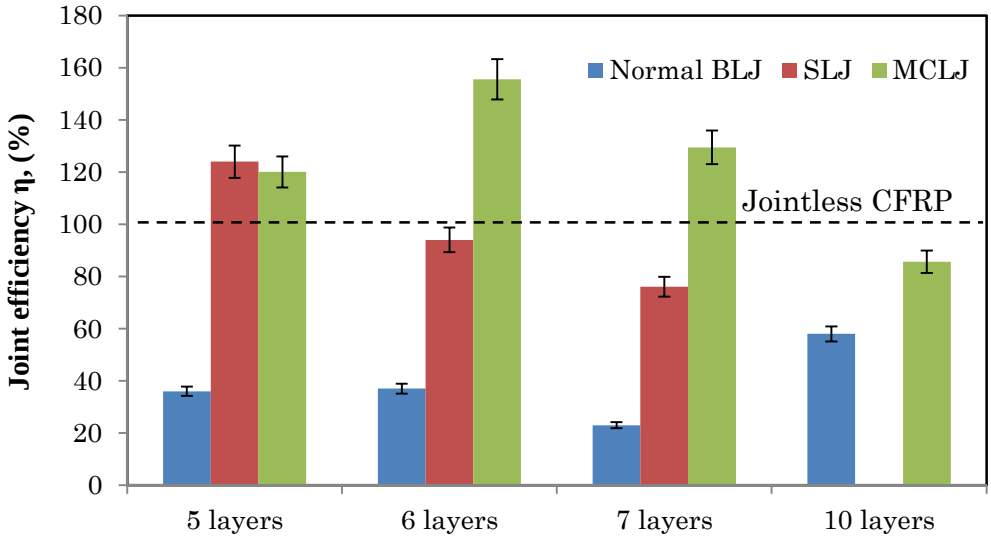

Figure 16. Joint efficiencies for the various laminate joints as compared with jointless CFRP

4. Conclusions

Laminated adhesive joints were made using the VARTM process. Three types of laminated joints were studied: BLJ, SLJ, and MCLJ. All joint specimens were tested under a three-point bending load to evaluate their strength performances in terms of nominal bending strength. For the normal BLJ, an increase in layers improved the bending strength, while a shifted layup formed a concave notch where a larger number of layers caused weaker bending strength. AE analysis and fractographic observation confirmed that the fracture mode for the normal BLJ consisted mainly in fiber breakages prior to the maximum load point, which dominated the bending strength mechanism of a

normal BLJ. A shifted layup in the joint caused that the fracture initiation mode was resin cracking at the notch site. SLJs showed a very improved bending strength compared to BLJs. The SLJ with 5 layers showed excellent joint efficiency, of around 124%. The MCLJ achieved superior bending strength, in which the joint efficiency for 5–7 layer joints exceeded 120%. The best efficiency among all the joint types was obtained with the 6-layer MCLJ. It was confirmed by combined AE and microscopic analysis that fiber breakages were significantly dominant, i.e., the fiber reinforcement caused a superior bending strength for the joint types of SLJ and MCLJ. Consequently, stitching and multiple-cover insertion clearly reinforced the adhesive joints, in which some optimal layup thickness and surface profile perfectness formed by the VARTM were required to show the best bending strength.

ACKNOWLEDGMENT

This work was partly supported by a research grant from the Japan Society for Promotion of Science (#JP26630496) and by the Collaborative Research Program of the Research Institute for Applied Mechanics, Kyushu University.

References

[1] Keller T, Vallée T. Adhesively bonded lap joints from pultruded GFRP profiles. Part I: stress-strain analysis and failure modes. Composites Part B 2005; 36: 331–340.
[2] Burns L, Mouritz AP, Pook D, Feih S. Strengthening of composite T-joints using novel ply design approaches. Composites Part B 2016;88: 73–84.
[3] Shufeng L, Xiaoquan C, Qian Z, Jie Z, Jianwen B, Xin G. An investigation of hygrothermal effects on adhesive materials and double lap shear joints of CFRP composite laminates. CompositesPart B 2016; 91: 431–440.
[4] Akderya T, Kemiklioğlu U, Sayman O. Effects of thermal ageing and impact loading on tensile properties of adhesively bonded fibre/epoxy composite joints. Composites Part B 2016; 95: 117–122.
[5] Abusrea MR, Arakawa K. Improvement of an adhesive joint constructed from carbon fiber-reinforced plastic and dry carbon fiber laminates. Composites Part B 2016;97: 368–373.
[6] Xiang J, Zhao S, Li D, Wu Y. An improved spring method for calculating the load distribution in multi-bolt composite joints. Composites Part B 2017; 117: 1–8.
[7] Friedrich C, Hubbertz H. Friction behavior and preload relaxation of fastening systems with composite structures. Composite Structures, 2014; 110: 335–341.
[8] Lee YH, LimDW, Choi JH, Kweon JH,Yoon MK. Failure load evaluation and prediction of hybrid composite double lap joints. Composite Structures 2010;92(12): 2916–2926.
[9] Oplinger JW. Mechanical fastening and adhesive bonding. In: Handbook of composites edited by Peters ST. Springer (New York) 1998.
[10] Abusrea MR, Jiang S, Chen D, Arakawa K Novel CFRP adhesive joints and structures for offshore application. International Journal of Chemical, Molecular, Nuclear, Materials and Metallurgical Engineering 2015; 9 (9): 1115-1118.
[11] Abusrea MR, Arakawa K. Evaluation of the strength of CFRP adhesive joints manufactured using VARTM. Advanced Experimental Mechanics 2016;1 : 111-114.
[12] Chen D, Arakawa K, Jiang S. Novel joints developed from partially un-moulded carbon-fibre-reinforced laminates. Journal of Composite Materials 2015; 49(14): 1777–1786.
[13] Ascione F. The influence of adhesion defects on the collapse of FRP adhesive joints. Composites Part B 2016 ;87: 291–298.
[14] Heim D, Hartmann M, Neumayer J, Klotz C. Ahmet-Tsaous Ö, Zaremba S, Drechsler K. Novel method for determination of critical fiber length in short fiber carbon/carbon composites by double lap joint. Composites Part B 2013; 54: 365–370.
[15] Akpinar S. The strength of the adhesively bonded step-lap joints for different step numbers. Composites Part B 2014; 67 : 170–178.

[16] Löbel T, Kolesnikov B, Scheffler S, Stahl A, Hühne C.. Enhanced tensile strength of composite joints by using staple-like pins: Working principles and experimental validation. Composite Structures 2013;106: 453–460.

[17] Mouritz AP, Chang P, Cox BN. Fatigue properties of z-pinned aircraft composite materials. ICAS Int Cong Aeronaut Sci 2006.

[18] Dransfield KA, Jain LK, Mai YW. On the effects of stitching in CFRPs—I. mode I delamination toughness. Composites Science and Technology 1998; 58(6): 815–827.

[19] Heß H, Himmel N. Structurally stitched NCF CFRP laminates. Part 1: Experimental characterization of in-plane and out-of-plane properties. Composites Science and Technology 2011; 71(5): 549–568.

[20] Kim JH, Park BJ, HanYW. Evaluation of fatigue characteristics for adhesively-bonded composite stepped lap joint. Composite Structures 2004; 66(1): 69–75.

[21] Mitsubishi Rayon CO., LTD., Profile Department, www.mrc.co.jp

[22] Yoon SY, Arakawa K, Han SW, Chen D, Choi NS. Effect of compaction treatment on laminated CFRP composites fabricated by vacuum-assisted resin-transfer molding. Polymer Composites. 2017; 38(2): 217-226.

[23] Gu JU, Yoon HS, Choi NS. Acoustic emission characterization of a notched aluminum plate repaired with a fiber composite patch. Composites Part A 2012; 43(12): 2211–2220.

[24] Budhe S, Banea MD, de Barros S, da Silva LFM.. An updated review of adhesively bonded joints in composite materials. International Journal of Adhesion and Adhesives 2017;*72*: 30–42.

[25] Ribeiro T, Campilho R, da Silva L,Goglio L. Damage analysis of composite–aluminium adhesively-bonded single-lap joints. Composite Structures 2016; 136: 25-33.

[26] Jensen EM, Leonhardt DA, Fertig RS. Effects of thickness and fiber volume fraction variations on strain field inhomogeneity. Composites Part A 2015 ;*69*: 178–185.

[27] Plain KP, Tong L. An experimental study on mode I and II fracture toughness of laminates stitched with a one-sided stitching technique. Composites Part A 2011; 42(2): 203–210.

[28] Velmurugan R., Gupta NK, Solaimurugan S, Elayaperumal A. The effect of stitching on FRP cylindrical shells under axial compression. International Journal of Impact Engineering 2004; 30(8): 923–938.

[29] Chung WC, Jang B Z, Chang T C, Hwang LR, Wilcox R CFracture behavior in stitched multidirectional composites. Materials Science and Engineering A 1989; 112: 157–173.

[30] Adanur S, Tsao YP. Stitch bonded textile structural composites. Proc. 26th Int. SAMPE Tech. Conf. (1994) pp. 25–34.

[31] Aymerich F, Onnis R, Priolo P. Analysis of the fracture behaviour of a stitched single-lap joint. Composites Part A 2005; *36*(5): 603–614.

[32] Sawyer JW. Effect of stitching on the strength of bonded composite single lap joints. AIAA Journal 1985; 23 (11): 1744-1748.

[33] Lalit KJ, Leong KH, Mai YW, Tong L. Effect of through-thickness stitching on the fatigue life of composite single-lap joints. Applied Composite Materials, 1998; 5 (6): 399-409.